ORIGINAL PAPER

A method to estimate maximum and minimum air temperature using MODIS surface temperature and vegetation data: application to the Maipo Basin, Chile

Eduardo Bustos · Francisco J. Meza

Abstract We present a method to estimate minimum and maximum air temperatures that uses land surface information from the Moderate Resolution Imaging Spectroradiometer (MODIS). The method is based on an analysis of the distribution of the Normalized Difference Vegetation Index (NDVI) and Land Surface Temperature (LST) obtained from the MODIS sensor. We select the pixels with high values of NDVI for each set of NDVI–LST images to represent vegetation pixels with adequate water conditions, ensuring that temperature values between surface and air surrounding are similar. Then, these pixels are spatially interpolated in order to obtain whole region maps of maximum and minimum air temperature. Estimates were compared with observed values for 12 meteorological stations distributed in the study area. After correcting for bias and lags between satellite and surface observation times, the majority of the stations show air temperature estimates that have no significant differences compared to the observed air temperature values. Except for urban areas, results show a correct representation of spatial and temporal distribution of maximum and minimum temperatures for all surface types.

1 Introduction

Air temperature is one of the most relevant variables to be considered in environmental studies (Geiger 1965). At

E. Bustos (✉) · F. J. Meza
Centro Interdisciplinario de Cambio Global, Pontificia Universidad Católica de Chile, Av. Vicuña Mackenna 4860, Macul, Santiago, Chile
e-mail: efbustos@uc.cl

F. J. Meza
Departamento de Ecosistemas y Medioambiente, Facultad de Agronomía e Ingeniería Forestal, Pontificia Universidad Católica de Chile, Av. Vicuña Mackenna 4860, Macul, Santiago, Chile

ecosystem scales, it influences the distribution of plant species (Cabrera 2002) and affects the dynamics of the soil–plant–water system (Chartzoulakis and Psarras 2005; Zavala 2004), being included in evapotranspiration models (Allen et al. 2006; Carlson et al. 1995) as well as hydrological models (Purkey et al. 2007; Yates et al. 2005). At the individual level, temperature affects plant growth and net primary productivity since photosynthetic and respiration rates depend on it.

Despite its relevance and the relative simplicity of measurement, air temperature data are not usually available with the desired spatial resolution for detailed regional analysis and/or their record length is sometimes insufficient for time domain characterization. For heterogeneous terrain, where we often observe different land cover types and changing topography, it is necessary to have a fairly dense network of observations to adequately represent a study area due to a lot of factors that are involved in air temperature dynamics (Geiger 1965).

Recognizing that this is a highly relevant and frequent problem, several methods have been developed to improve time–space estimation of air temperature. Some of them consider land topography as a relevant variable and develop different algorithms for spatial interpolation using geographic features as independent variables (Chuanyan et al. 2005; Colombi et al. 2007; Dodson and Marks 1997; Jarvis and Stuart 2001; Lookingbill 2003). A second set of methods use satellite images to model spatial behavior of temperature using energy budget theory (Nieto et al. 2011; Prihodko and Goward 1997; Stisen et al. 2007). Since surface temperature is the result of energy balance and ultimately of the ratio between latent and sensible heat, we can explore the relationship between surface temperature and plant water status to characterize the spatial distribution of air temperature in a given landscape.

The thermal characteristics of the atmospheric layer closest to the surface can be inferred from surface temperature (T_s),

considering the characteristics of the vegetation cover and water status (Geiger 1965). Such interactions have been applied in the past (see Jackson (1981) for a summary) to characterize plant water status and develop tools to schedule irrigation based on the differences between air temperature (T_a), the canopy temperature (T_c), and soil water availability (Jackson et al. 1988; Jackson 1981; Jackson et al. 1981). Ehrler et al. (1978) related temperature differences between surface cover and the adjacent air (ΔT) to plant water potential (ψ_{plant}), finding a negative relationship between these two variables, which is explained by variations in soil moisture at root level, which influences canopy resistance. When available water is reduced, stomatal closure is observed, favoring sensible heat flow and causing temperature rise.

The development of remote sensing information has made possible to enable simultaneous surveys of surface temperature and spectral response in visible and near-infrared regions of the spectrum, capturing spatial and temporal variations of both the plant cover (expressed as the normalized difference vegetation index, NDVI; Pettorelli et al. 2005) and its temperature, T_s. The relationship between both variables has been widely used in several applications: characterization of the temporal variation and relationship between LST and vegetation characteristics among platforms/sensors (Goetz 1997), development of a crop water deficit estimation (Moran et al. (1994), determination of regional evapotranspiration (Batra et al. 2006; Carlson et al. 1995; Stisen et al. 2008), estimation of soil moisture (Gillies et al. 1997; Gillies and Carlson 1995; Sandholt et al. 2002), and calculation of canopy resistance to evapotranspiration (Blonquist et al. 2009; Nemani and Running 1989).

For a particular land cover, the slope between NDVI and T_s has also been related to the rate of evapotranspiration (Prihodko and Goward 1997). Jackson et al. (1981, 1988) and Nemani and Running (1989) have shown that the physical relationship between NDVI and T_s is explained by the different sensitivities of canopy and soil surface to changes in soil moisture because it affects thermal characteristics of coverage, as well as the ratio of latent to sensible heat fluxes (Prihodko and Goward 1997; Stisen et al. 2008). In this process, we should also consider factors such as evapotranspiration rates, the thermal properties of the surface, the available net radiation, wind velocity, and surface roughness because they modify the rate of energy and matter exchange between the surface and atmosphere, which determine the relative position of a pixel within the NDVI–T_s space (Sandholt et al. 2002). This response is much higher in bare soils than in dense canopies (Gillies and Carlson 1995) and is very sensitive to variations in soil and vegetation type (Gillies et al. 1997; Sandholt et al. 2001).

Thus, for normal values of aerodynamic resistance, the magnitude of evapotranspiration flux and subsequent cooling of the surface increases with the resistance reduction and is promoted by higher water availability. Potential latent heat flow depends on the available net radiation and magnitude of vapor pressure deficit. The resistance depends on both wind speed and the surface roughness (Jones 1992). These dependencies and interactions hinder the analysis of the results obtained by different estimation methods (Sandholt et al. 2002).

The interpretation of the surface temperature for open canopies, such as the case of sclerophyllous shrubs, presents the additional difficulty that the temperature measurements are composed by thermal signals coming from both the bare soil and the existing vegetative cover.

The relationships between NDVI and T_s determined that, for the domain considered, areas with high vegetation cover (i.e., areas with higher NDVI values) correspond to areas where a minimum amount of the emitted radiation comes from the soil, and we can associate the temperature recorded by the sensor (T_s), with the temperature of the cover (T_c) (Jackson et al. 1988). This can be seen in a scatter plot between NDVI and T_s value of all pixels considered (Fig. 1), where it is seen that the observations have a triangular (Gillies and Carlson 1995) or trapezoidal distribution (Moran et al. 1994), which represents the value ranges of all NDVI and T_s combinations at the time of image acquisition.

Canopies with high values of NDVI represent dense covers and therefore present a structure that maximizes heat diffusion effect (Gates 1968; Geiger 1965), allowing thermal equilibrium with the adjacent air. Consequently, it is possible to consider that the surface temperature of those pixels is a good approximation of the air temperature at the time of image acquisition (Nieto et al. 2011; Stisen et al. 2007).

The main hypothesis of this work is that the information available in MODIS surface temperature and NDVI images allow us to determine the variability of surface temperature and vegetation considering all land cover types present. Assuming that the temperature of dense ground cover located at
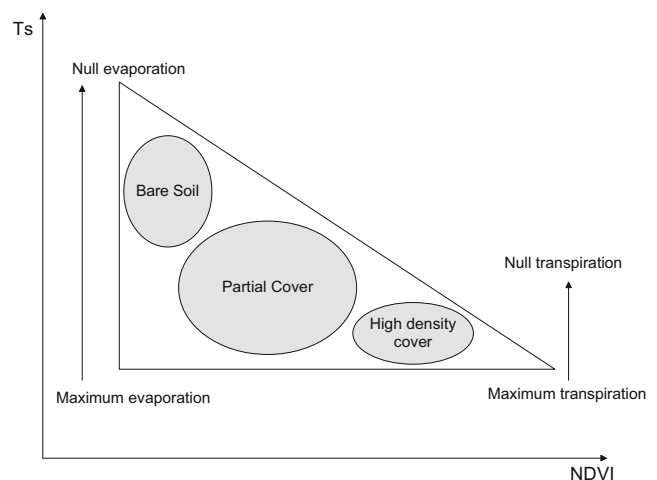

Fig. 1 Simplified representation of the ratio Ts/NDVI according to the degree of vegetation cover (adapted from Sandholt et al. (2002))

high values of NDVI in the NDVI– T_s distribution is very close to the air temperature, it is possible to obtain a good estimate of air temperature, which is a very useful approximation to improve the spatial distribution of air temperature in a regional scale.

Therefore, the main objective of this study is to develop a methodology to obtain an estimate of the near-surface air temperature using information from satellite images in the visible, near-infrared, and thermal infrared spectra.

2 Materials and methods

2.1 Study area

The study area considered corresponds to the Maipo River Basin located in central Chile between latitudes 32°55′ and 34°15′ S. The area covers a total of 15,317 km², of which one third corresponds to mountainous terrain. The altitude profile of the basin extends from 0 to 6,500 m from the mouth of the Maipo River in the Pacific Ocean to the border with Argentina in the Andes, with an average elevation of 1,660 m. The region has an important watershed area above 2,000 m in elevation. Topographically, there are four important elements from east to west: Andes, Central Valley, Coast Range, and Coastal Plains. According to the Meteorological Office of Chile (DMC), there are two climate subtypes in this region: a temperate Mediterranean type with a long dry season and a temperate Mediterranean type with a dry season of 4 to 5 months. The latter is influenced by the height of the Andes (Fig. 2).

The main vegetation types in the study area are the sclerophyll forest, deciduous forest, and tree-thorn shrub, which vary in proportion to the interior of the basin (Luebert and Pliscoff 2006). The basin is characterized by fairly large agricultural and urban areas (Table 1; Fig. 3). Nevertheless, the predominant land cover types below 2000 m are the thorn shrub with open grasslands and agricultural land (Muñoz-Schick et al. 2000).

Due to the effect of topography over temperatures of air masses related to the adiabatic lapse rate (Colombi et al. 2007; Dodson and Marks 1997; Geiger 1965), we consider as study area the basin area below 2,000 meters for implementation of the method as well as discussion of results.

2.2 Weather information

Air temperature data were obtained from the network of weather stations of the Dirección General de Aguas (DGA) and the Dirección Meteorológica de Chile (DMC). We selected 12 stations within the basin and extracted maximum and minimum temperatures throughout the study period (Jan 2004–Dec 2005). Figure 3 shows the spatial distribution of

meteorological stations considered, while Table 2 details the characteristics in terms of dominant land use in the locality where they are located.

2.3 MODIS images

We selected 47 pairs of MODIS images of good quality from the repository of the Geological Survey (USGS) and the Agency's National Air and Space Administration (NASA) (https://lpdaac.usgs.gov/) between Jan/1/2004 and Dec/31/2005 for a daily temporal resolution at 1 km of spatial resolution in LST images (MYD11A1—day/night) and 16 days and 1 km for vegetation index product (MYD13A2—NDVI). We used standard processing level 3 (L3) data to ensure correct spatial concordance between the two images (Justice et al. 1998). As a proxy for vegetation cover characteristics, we used NDVI values since the absorption and reflectivity of the vegetation cover are correlated with their structural properties, such as the index leaf area (LAI), fractional vegetation cover (Fr), biomass, as well as their physiological condition (Huete et al. 2002; Jiang et al. 2006). This is explained by the particular spectral behavior of vegetation cover, with a high absorption of red (approximately 650 nm) by chlorophyll and the high reflectivity of the mesophyll of the leaf to the near-infrared (approximately 850 nm). Values of NDVI vary between −1 and 1, where the range between 0.2 and 0.9 is the most common in continuous vegetation cover (Huete et al. 2002).

$$\text{NDVI} = \frac{\rho\text{NIR} - \rho\text{Red}}{\rho\text{NIR} + \rho\text{Red}} \tag{1}$$

where ρNIR is the near-infrared reflectance (841–876 nm) and ρRed the reflectance of the red band (620–670 nm).

The land surface temperature (LST) is obtained from the emissivity of MODIS bands 31 (10.780–11.280 μm) and 32 (11.770–12.270 μm). Their respective radiances were obtained using the split-window algorithm developed for the MODIS LST product (Wan et al. 2002; Wan and Dozier 1996; Wan and Li 1997), which corrects for atmospheric effects and emissivity using a lookup table based on global land surface emissivity in the thermal infrared (Snyder et al. 1998).

The *Aqua* platform was regarded as the most appropriate since its time of observation over the study area roughly correspond with the moment when the highest temperatures are usually observed (13:30 local time). The time of observation at night occurs around 1:30 local time. Although it does not match the moment when minimum temperatures are usually observed, we consider this estimate a fairly reasonable approximation, which will be corrected for daily minimum temperature estimation.
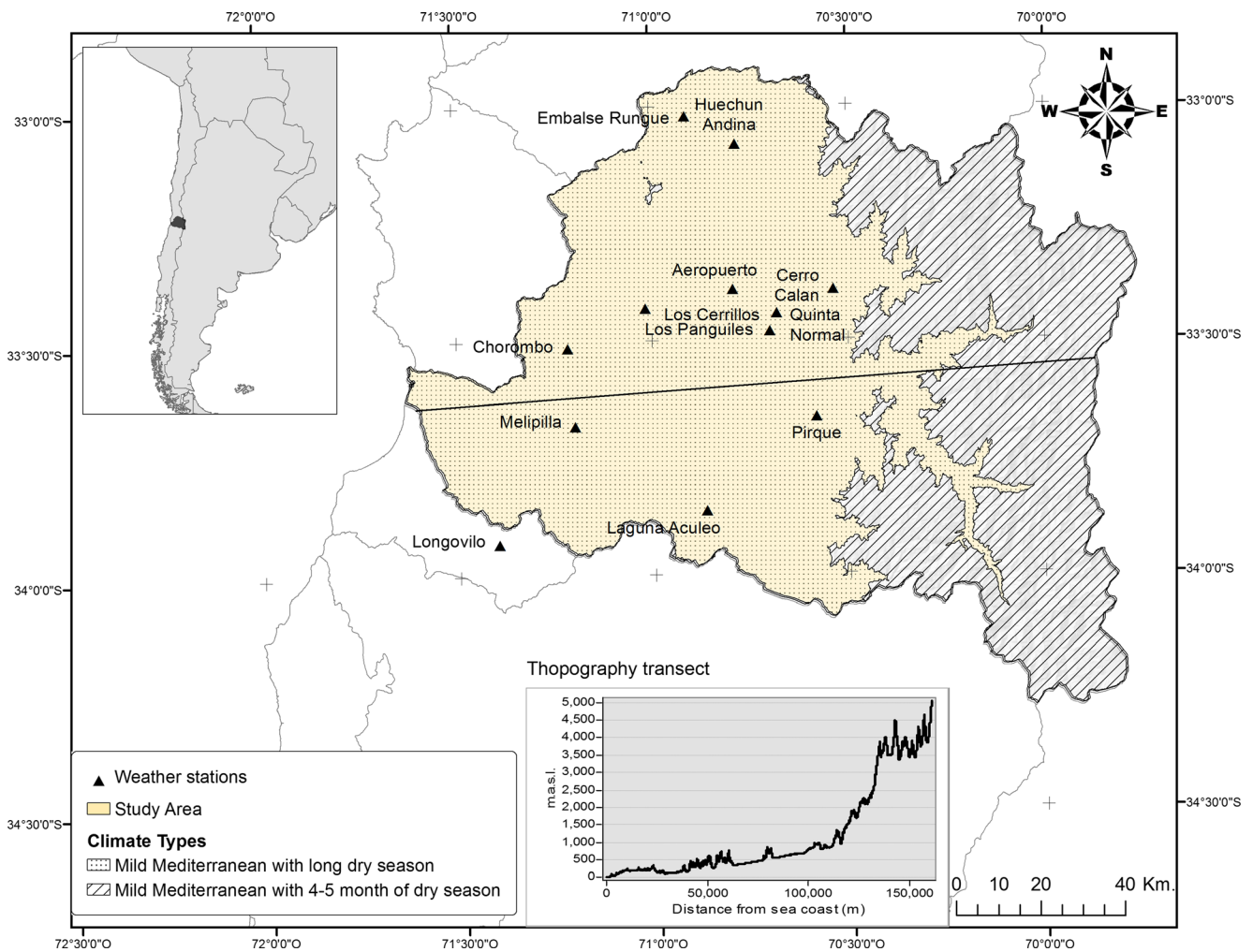
Fig. 2 Study area and spatial distribution of weather stations. It also presents the altitude profile and the distribution of climates in the region

The LST images from MODIS were filtered using quality flags of the product, keeping only the pixels classified as good quality in order to ensure using reliable information about surface temperature.

Table 1 Area and land use percentage as in the Maipo River Basin

Land use	Area (km^2)	%
Grassland and shrub	6,938.4	45.50
Bare soil	3,811.0	24.99
Agricultural land	2,532.4	16.61
Urban and industrial areas	837.0	5.49
Forest	820.5	5.38
Plantations	101.9	0.67
Snow and glaciers	87.7	0.58
Wetlands	68.7	0.45
Water bodies	51.8	0.34
Total	15,249.3	100

2.4 Air temperature estimation based on MODIS NDVI and LST

For the estimation of maximum and minimum air temperature, we implemented the following protocol and applied it to all images (Fig. 4):

- We selected pixels with the highest values of NDVI defined as those which showed values equal or greater than the 90th percentile in each data set. This criterion was selected because other parametric thresholds would be difficult to achieve as NDVI usually has non-normal distributions. This threshold was chosen because it produced a reasonable balance between the number of pixels selected and a theoretically valid value of NDVI. Based on selected pixels, we built a mask layer to extract corresponding surface temperature values from the LST image. From this temperature data, we removed outliers (mean plus 2.5 standard deviations).
- We then interpolated the data to generate a surface of temperature estimates. The interpolation procedure was
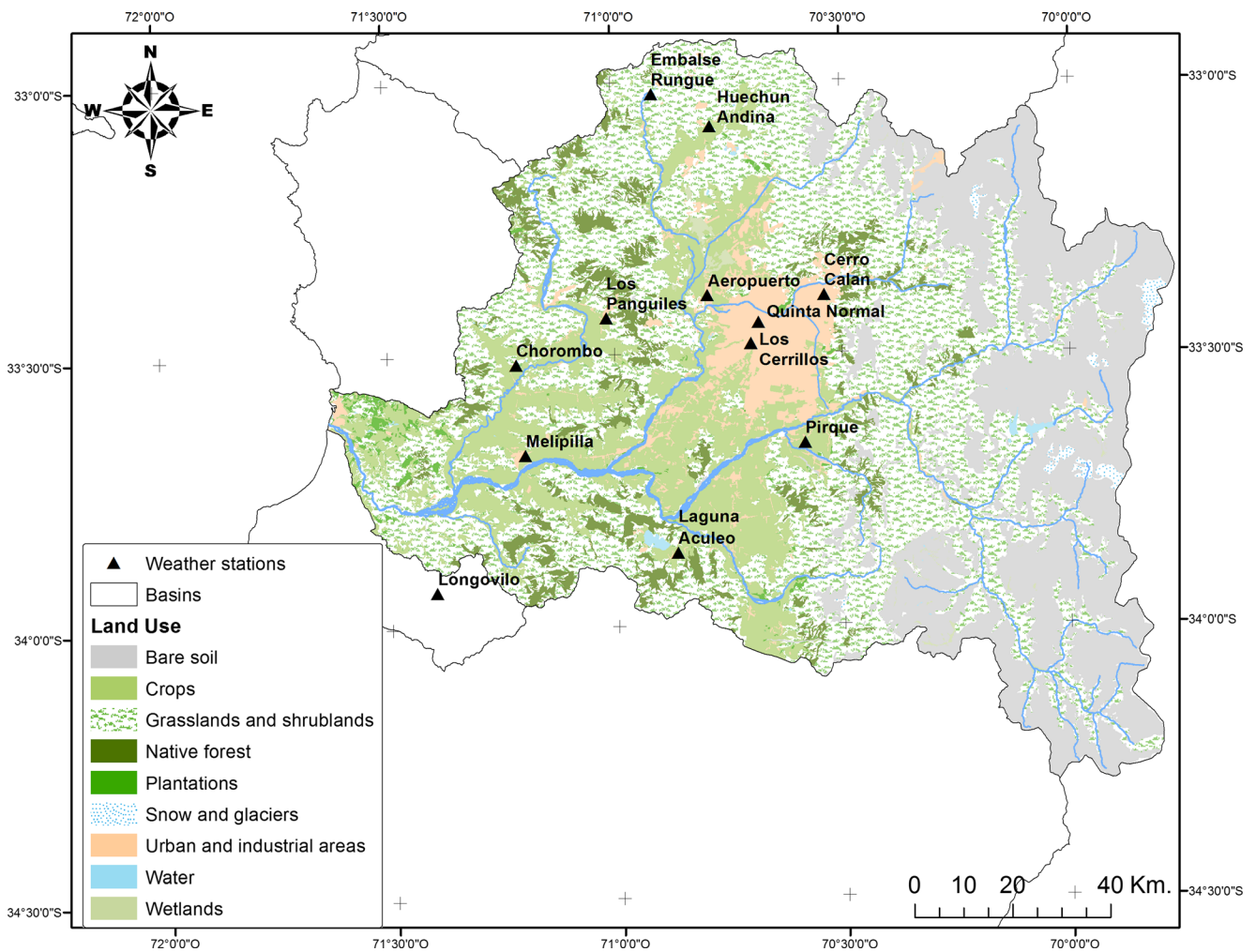
Fig. 3 Land use in the watershed of the Rio Maipo. Highlighted is the large amount of land used for agriculture and urban characteristics

carried out using the inverse distance weighted method (IDW) since previous studies indicate that it reduces

computational time and produces similar results in terms of accuracy in relation to geostatistical procedures

Table 2 Weather stations of the study, with geographical coordinates, altitude, and land cover associated

Station	Localization			Land use
	Longitude	Latitude	Altitude (m)	
Aeropuerto	−70°47′	−33°23′	475	Urban and industrial areas
Cerro Calán	−70°32′	−33°23′	800	Urban and industrial areas
Chorombo	−71°13′	−33°31′	140	Agricultural land
Huechún Andina	−70°47′	−33°5′	580	Grassland and scrubs
Laguna Aculeo	−70°52′	−33°52′	360	Agricultural land
Longovilo	−71°24′	−33°56′	140	Agricultural land
Los Cerrillos	−70°42′	−33°29′	510	Urban and industrial areas
Los Panguiles	−71°1′	−33°26′	195	Grassland and scrubs
Melipilla	−71°12′	−33°41′	165	Agricultural land
Pirque	−70°35′	−33°40′	670	Agricultural land
Quinta Normal	−70°40′	−33°26′	520	Urban and industrial areas
Embalse Rungue	−70°54′	−33°1′	700	Grassland and scrubs

Fig. 4 Diagram of methodology
for air temperature estimation
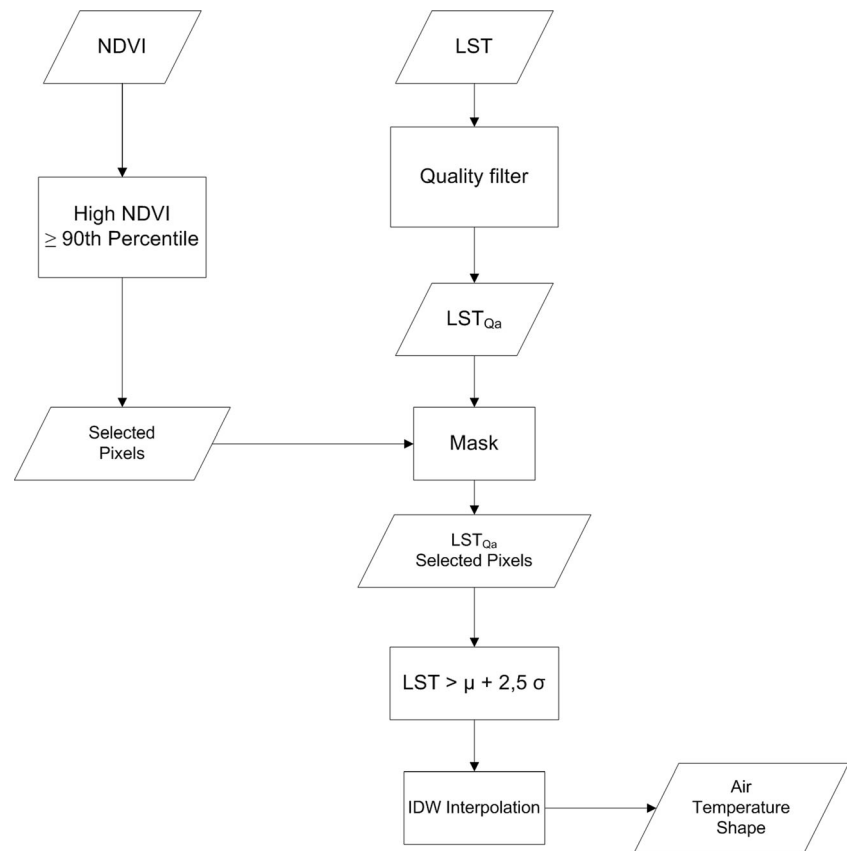
(Chuanyan et al. 2005; Jarvis and Stuart 2001; Li and
Heap 2008). Details of this procedure are provided in the
following section.

We compared the estimates of minimum and maximum
temperature with observed values of the 12 weather stations.
To obtain the maximum temperatures, it was necessary to
correct for bias in the modeled values. We calculated monthly
bias for each land cover type and concluded that seasonal
variability of maximum temperature bias was far more impor-
tant than land cover variability. Minimum temperatures on the
other hand showed comparatively less temporal variability
with almost no dependence on land cover.

For this reason, we applied an empirical correction
throughout the year. In the case of maximum temperature,
we fitted a polynomial (Eq. 2), whereas in the case of mini-
mum temperature we only subtracted the mean bias:

$$T_{\text{max-bias}} = -1.4958M - 0.1556M^2 + 0.0233M^3 + 11.888 \quad (2)$$

2.5 Spatial interpolation of air temperature estimations

The IDW method estimates the value of an attribute at the
point of interest using a linear combination of the known
values, weighted by the inverse function of the distance

between known points and the point considered. This method
indicates that highest weights are given to the nearest points
because their values can be regarded as more similar to the
values found in a desired point or station (Li and Heap 2008).

The relation is:

$$\lambda_i = \frac{n/d_i^p}{\sum_{i=n}^{n} n/d_i^p} \quad (3)$$

where d_i is the Euclidean distance, based on x, y, and z
coordinates, between the know values and the point of inter-
est, p is the power parameter, and n is the number of points
included in the estimation (neighbors). For this method, the p
parameter is directly related to the influence of the closest
points to interpolated point; high p values imply local behav-
ior of the variable, while low values are associated to a more
regional behavior of the variable. In this case, we used $p=2$
and the 11 closest neighbors, which allows for the use of this
method for all of the observation dates. In locations of com-
plex terrain, altitude is a variable that influences climatic
conditions. Recognizing the relevance of height, to calculate
distance, we modified weights and give the vertical distances a
value of 1.5 in comparison to horizontal ones. This resulted in
improved estimations of temperature. For both estimates of
the maximum and minimum air temperatures, mean values

and corresponding errors are reported (difference between modeled air temperature and meteorological station). In addition, we report the mean square error obtained after cross-validation. These indices are a measure of the quality of the interpolation and its reliability in the region under study where there are not many validation points for the observed values of air temperature.

For maximum and minimum temperature estimates, we calculated a set of indicators in order to evaluate the validity of the model. Mean and standard deviation were calculated, as well as the root mean square error (RMSE) and the correlation coefficient (r) to evaluate the model results with respect to the observed values. All statistical analyses were performed using the open source software R (R Development Core Team 2012).

3 Results

3.1 Maximum air temperature estimation

3.1.1 Mean values of maximum temperature estimation

The estimation method was applied to the whole set of MODIS images. Table 3 shows the statistics of the air temperature estimations for each reference weather station.

There is a good representation of the general patterns for the study area, with average differences of 4.26 °C compared to the observed air temperature data. This difference corresponds to an overestimation of the method for all stations considered, with values ranging between 6.3 and 1.1 °C above the actual values for stations Aeropuerto and Laguna Aculeo, respectively.

With these results, we determine that the method presented for the case of estimated maximum air temperatures widespread bias of 4.25 °C. This is explained because the selected ground cover, despite having a good water supply and therefore low surface temperatures, had a temperature higher than the values recorded by the stations. This can be explained by the high water demand which could lead to water stress and therefore would trigger stomatal closure processes in the leaf, which are responsible for an increase in leaf temperature (Vitale et al. 2007; Zavala 2004). This therefore determines the surface temperature of the cover which is, for daylight satellite overpass, systematically higher than measured air temperatures.

In order to improve the estimation accuracy, a bias correction was applied using values from Eq. 2. The new results are shown in Table 4.

With respect to the variability of estimated air temperature relative to that observed at all weather stations, we observe that the estimates represent the seasonal patterns of air temperature. There is a difference of 2.99 °C between the observed and modeled values. The largest difference is at Pirque station, with 4.02 °C, while the smallest difference of 0.96 °C is found at Longovilo station. Figure 5 shows, for five weather stations of the study, box plots for the distribution of observed and modeled values.

The correction of bias for the maximum temperatures adjusts the measures of central tendency estimates, keeping the variability obtained through the calculation process (Fig. 5). This approach has been used in other similar studies (Dodson and Marks 1997; Prihodko and Goward 1997).

The distribution of modeled and observed maximum air temperature values shows root mean square errors exceeding on average 6.82 °C, reaching 8.36 °C as the maximum value in Huechún Andina station. These values are higher than other

Table 3 Summary table with modeled maximum air temperature values (Mod) against observed values (Obs) and its difference (Dif=Mod-Obs), for mean (ME), and standard deviation (SD). In addition, the root mean square error (RMSE) and the correlation coefficient (r) between the observations and the estimated values for each weather station for the entire set of images (n=47)

Weather station	ME			SD				
	Obs	Mod	Dif	Obs	Mod	Dif	RMSE	r
Aeropuerto	24.04	30.43	6.39	5.97	9.47	3.49	8.26	0.74
Cerro Calán	24.70	29.16	4.46	6.19	9.71	3.53	7.19	0.69
Chorombo	23.36	25.84	2.49	6.11	7.73	1.62	4.87	0.70
Huechún Andina	24.62	30.60	5.98	7.12	9.78	2.67	8.36	0.63
Laguna Aculeo	24.81	25.95	1.14	5.82	9.32	3.50	5.54	0.69
Longovilo	22.64	25.72	3.08	6.8	7.76	0.96	5.43	0.66
Los Cerrillos	24.70	30.11	5.41	5.92	9.12	3.21	7.45	0.71
Los Panguiles	23.56	27.50	3.93	6.13	8.81	2.68	5.92	0.77
Melipilla	23.16	27.36	4.21	5.56	9.04	3.48	6.73	0.70
Pirque	24.11	28.37	4.26	5.83	9.86	4.02	7.64	0.60
Quinta Normal	23.80	29.99	6.19	6.1	9.36	3.25	8.29	0.67
Embalse Rungue	25.42	28.97	3.56	6.16	9.63	3.46	6.14	0.78
Average	24.08	28.33	4.26	6.14	9.13	2.99	6.82	0.69

Table 4 Mean value of maximum observed and modeled air temperatures (°C) after bias correction for each weather station

Weather station	Maximum temperature	
	Obs	Mod-bias
Aeropuerto A.M.B.	24.04	27.37
Cerro Calán	24.70	26.10
Chorombo	23.36	22.79
Huechún Andina	24.62	27.54
Laguna Aculeo	24.81	22.89
Longovilo	22.64	22.66
Los Cerrillos	24.70	27.05
Los Panguiles	23.56	24.44
Melipilla	23.16	24.30
Pirque	24.11	25.31
Quinta Normal	23.80	26.93
Embalse Rungue	25.42	25.91
Average	24.08	25.27

methods for estimating air temperature, where the RMSE values are between 1 and 3 °C for similar heterogeneous conditions (Kawamura and Edamatsu 1993; Stisen et al. 2007; Yan et al. 2009), as in mountain ranges (Colombi et al. 2007). Nevertheless, the correlation coefficients are relatively high for the modeled air temperature estimates for all stations, showing an average value of 0.69, with values ranging between 0.60 and 0.78. This reflects that a major portion of the variable behavior is being captured by this method.

We conducted a *t*-test using the observed and unbiased modeled data for each weather station to examine if there were significant differences. The null hypothesis is that there were no differences between them. Because the data exhibit the phenomenon of temporal autocorrelation of first order, both for the observed and estimated data (Table 5), we applied the *t*-test for autocorrelated data, which applies an inflation factor of variance in the calculation of the p-value (for details, see Wilks (2005)).

Fig. 5 Distribution of observed values, biased estimation, and unbiased estimations of maximum temperature. The *horizontal line of each box* is the median value of a data set, and the *upper* and *lower limits of a box* are the third and fourth quantile. The *ends of the dotted lines* are the range of values for each data set
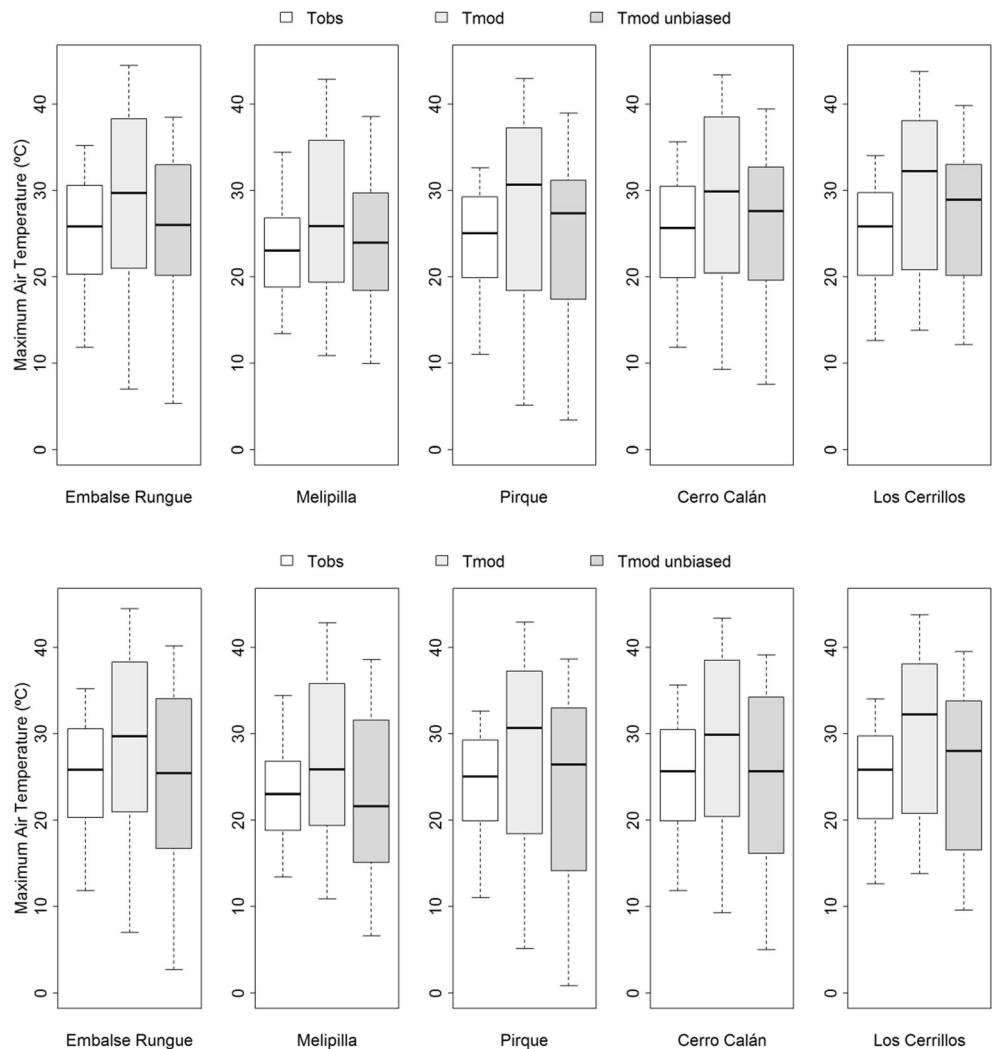
Table 5 First order autocorrelation coefficients (r1) for observed and estimated maximum temperatures and *p* values for *t*-test. Italicized values indicate rejection of the null hypothesis of equal mean values with 95 % confidence interval

Weather stations	Autocorrelation coefficients		
	Obs	Est	*p* value
Aeropuerto	0.60	0.75	*0.00*
Cerro Calán	0.58	0.73	0.08
Chorombo	0.73	0.74	0.72
Huechún Andina	0.73	0.71	*0.00*
Laguna Aculeo	0.62	0.68	0.97
Longovilo	0.64	0.75	0.49
Los Cerrillos	0.56	0.78	*0.01*
Los Panguiles	0.74	0.79	0.19
Melipilla	0.67	0.73	0.13
Pirque	0.50	0.68	0.11
Quinta Normal	0.55	0.77	*0.00*
Embalse Rungue	0.65	0.74	0.31
Average	0.63	0.74	

The *t*-test results revealed that for only three of the 12 stations considered in the study was there sufficient evidence to reject the null hypothesis about equality between observed values and estimates with 95 % confidence interval. These results suggest that, in regional terms and considering the heterogeneity of the placement of weather stations, the method allows to obtain estimates that are not statistically different from the observations recorded by weather stations in the Maipo River Basin.

One aspect that could be affecting the estimation of maximum and minimum air temperatures that cannot be quantified by this method is advection processes that disrupt the thermal balance conditions between the layers of air present at a given time (Campbell and Norman 1998; Geiger 1965; Li and Yu 2007). In this case, for the regional scale of this study, we have to assume conditions of stability and absence of advection.

3.1.2 Interannual variation of maximum air temperature estimations

The temporal behavior of the estimates is variable throughout the year for maximum temperatures (Fig. 6). There is a seasonal variability that responds to changes in both vegetation cover in the region and seasonal variations in air temperature. For the maximum temperatures seen in a good representation of seasonality, identifying fluctuations occurred in the study period. Also, the method shows the times of the year in which the estimates have particular behavior as observed during periods of overestimation of method occurred in the summer. On certain occasions, like mid spring, vegetation suffers rapid changes and a window of 16 days could not be the most

appropriate way to capture changes and represent temperature variations. For those cases, an 8-day NDVI product could be used.

It is possible to distinguish that uncorrected air temperature estimations have higher discrepancies in the summer months (December–January–February) with respect to a better fit that can be observed in the winter months (June–July–August). This overestimation is likely due to the behavior of the vegetation cover when high air temperatures and low soil moisture conditions occur (Duffkova 2006), where, as a Mediterranean ecosystem response, there is a decrease in gas exchange rate levels of stomata, which added a high vapor pressure deficit (Ehrler et al. 1978; Jackson et al. 1981), causing a decrease in vapor flows at the canopy level (Vitale et al. 2007). Ultimately, it implies a decrease in the rate of assimilation of carbon and an increase in surface temperature.

3.2 Minimum air temperature estimation for weather stations

3.2.1 Mean values of minimum temperature estimation

We calculated minimum air temperatures following the method presented here; the results are shown in Table 6.

For the case of minimum air temperature, the differences between estimated and observed data are quite low compared to the maximum temperatures. In this case, the average for all weather station differences is 1.11 °C, with extreme values of 2.99 °C at Rungue Embalse station and −1.15 °C at the Cerro Calan station. In the case of the urban stations (Cerro Calan, Los Cerrillos, and Quinta Normal), minimum temperatures have modeled the major differences from those observed, which might be related to the heat island phenomenon. This effect is observed in urban coverages and has the effect over rise observed temperature compared to non-urban environment, especially evident in atmospheric calm conditions and clear skies in nights, when the minimum temperatures are estimated. At this moment, the differences between radiative cooling of urban coverage and non-urban surroundings become more evident. (A very good description of these urban heating processes is provided by Voogt and Oke (2003).)

The model was able to represent the variability of the temperature. The observed differences represented by the estimated standard deviation of 0.38 °C averaged over all seasons, varying between 1.15 °C and −0.69 °C (Fig. 7).

The time of satellite observation may be a source of additional error in the model. In our case, nighttime observations occur between 1 and 2 AM, whereas it is known that observed minimum temperatures typically occur right before sunrise. One may want to correct this and fit a function that reproduces nighttime cooling in order to generate an adjusted value of satellite estimation (see an example of such functions in Campbell and Norman (1998)). In our case, such correction did not add any significant improvement to minimum
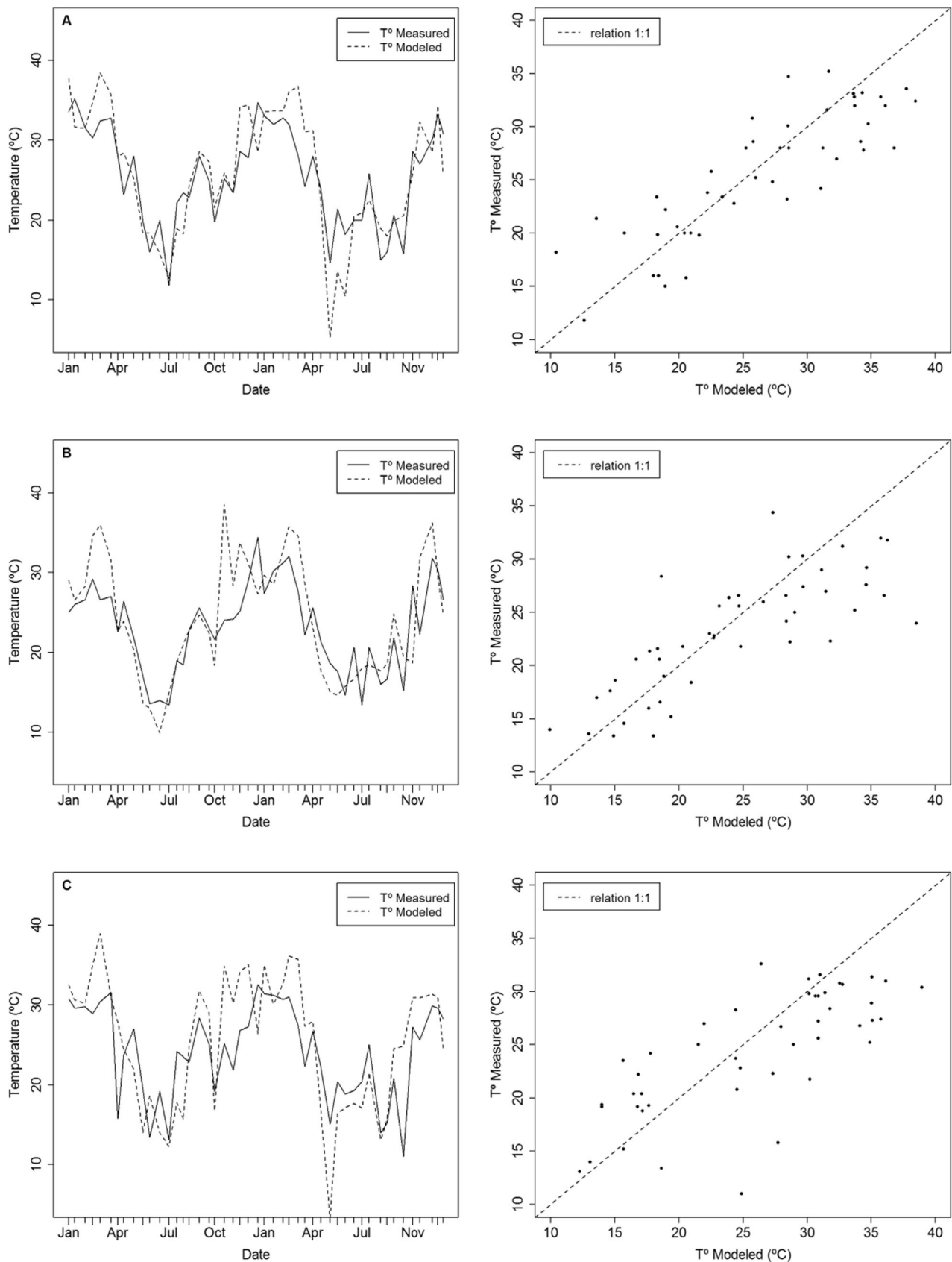
Fig. 6 Temporal distribution of maximum air temperature and the dispersion of estimated and observed temperature values for three weather stations: **a** Rungue Embalse, **b** Melipilla, and **c** Pirque. The 1:1 *line* shows the dispersion for each data set

Table 6 Summary table with modeled minimum air temperature values (Mod) against observed values (Obs) and its difference (Dif=Mod-Obs), for mean (ME), and standard deviation (SD). In addition, the root mean square error (RMSE) and the correlation coefficient (*r*) between the observations and the estimated values for each weather station for the entire set of images (*n*=47)

Weather station	ME			DE				
	Obs	Mod	Dif	Obs	Mod	Dif	RMSE	*r*
Aeropuerto	7.22	8.37	1.15	3.93	4.54	0.62	3.80	0.64
Cerro Calán	10.13	8.58	−1.55	3.75	4.29	0.54	3.60	0.67
Chorombo	5.55	8.12	2.57	3.69	3.80	0.11	3.67	0.75
Huechún Andina	6.21	8.50	2.29	4.95	4.64	−0.32	3.28	0.88
Laguna Aculeo	5.40	8.37	2.97	3.97	3.96	−0.01	4.08	0.75
Longovilo	6.84	8.37	1.53	2.95	3.98	1.03	3.72	0.55
Los Cerrillos	8.76	8.35	−0.41	4.03	4.39	0.36	3.01	0.75
Los Panguiles	8.27	8.19	−0.08	3.57	3.94	0.38	2.22	0.83
Melipilla	7.89	8.39	0.50	2.97	3.99	1.01	3.62	0.49
Pirque	6.62	7.93	1.30	3.44	4.59	1.15	4.06	0.56
Quinta Normal	8.41	8.45	0.04	3.98	4.35	0.37	3.20	0.70
Embalse Rungue	5.95	8.94	2.99	5.17	4.47	−0.69	3.99	0.86
Average	7.27	8.38	1.11	3.87	4.25	0.38	3.52	0.70

Fig. 7 Distribution of observed values (*Tobs*) and estimated values (*Tmod*) unbiased estimations of mínimum air temperatures. The *horizontal line* of each *box* is the median value of a data set, and the *upper and lower limits of a box* are the third and fourth quantile. The *ends of the dotted lines* are the range of values for each data set
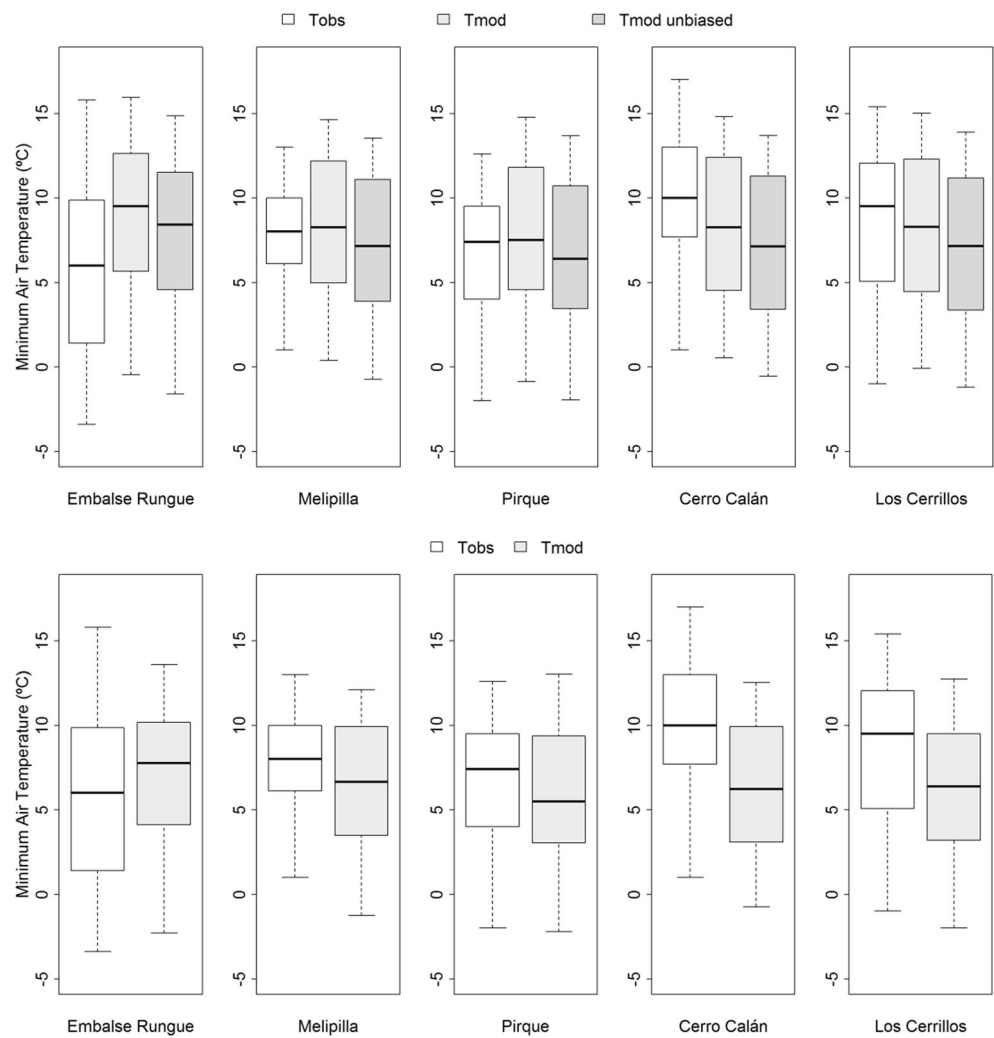
temperature estimates (results not shown) but can be considered as an avenue to explore in cases where nighttime cooling produces abrupt changes in temperature between satellite observation times the moment when minimum temperatures are typically observed.

As in the case of maximum temperatures, the value of RMSE is maintained with an average value of 3.58 °C for all seasons, varying between 2.22 and 4.08 °C at stations Los Panguiles and Laguna Aculeo, respectively.

The results obtained in *t*-test shows that four of the 12 stations have sufficient evidence to reject the null hypothesis about equality between observed values and estimates with a 95 % confidence interval, concluding that the remaining eight stations do not have enough evidence to say that the modeled data differ from the recorded weather station data (Table 7).

3.2.2 Interannual variation of minimum air temperature estimations

Estimates of the minimum air temperatures show a good representation of seasonal patterns, matching observed annual cycles in temperature (Fig. 8). However, the setting of the series of daily values has not been appropriately adjusted between modeled values which are significantly different from the minimum air temperature observations. This is mainly in the extreme values as opposed to results of other studies that use integrated average temperatures (Vancutsem et al. 2010).

Table 7 First-order autocorrelation coefficients (r1) for observed and estimated minimum temperatures and *p* values for *t*-test. Italicized values indicate rejection of the null hypothesis of equal mean values with 95 % confidence interval

Weather station	Autocorrelation coefficients		
	Obs	Est	*p* value
Aeropuerto	0.41	0.80	0.13
Cerro Calán	0.54	0.74	0.94
Chorombo	0.47	0.76	*0.01*
Huechún Andina	0.80	0.75	*0.01*
Laguna Aculeo	0.71	0.70	*0.00*
Longovilo	0.40	0.79	0.06
Los Cerrillos	0.63	0.80	0.66
Los Panguiles	0.64	0.73	0.53
Melipilla	0.20	0.79	0.31
Pirque	0.38	0.78	0.10
Quinta Normal	0.50	0.80	0.48
Embalse Rungue	0.77	0.72	*0.00*
Average	0.54	0.76	

It may be noted that the methodology of setting minimum temperatures has an additional adjustment by the correction from satellite images time to daily minimum temperature time. This has a significant effect in decreasing temperatures, forcing corrected temperatures to be significantly lower than observed.

Using geostatistical processing tools, we generated regional estimate maps of minimum and maximum temperature. Figure 9 shows the average temperatures observed for the months of January and July 2004–2005. The method proved to be valid only below 2,000 m.a.s.l., which corresponds to the altitudinal limit of ground cover (from vegetation to bare soil) needed for this methodology.

The methodology allowed distinguishing spatial patterns of temperature distribution. In the case of maximum air temperature, for both summer and winter seasons, the northern part of the basin showed consistently higher temperatures. This is a characteristic pattern of this region. The south and west areas of the basin present a temperature distribution explained by seasonal changes of coverage present in those sectors. These sectors are dominated by agriculture and shrubland areas which have high seasonal variations. Also, the topography influenced some sectors, showing warmer valleys in summer with the lowest temperatures in winter. The west margin of the study area has influence of the sea, with more temperate areas with minimum temperatures higher and maximum lower than the eastern and northern areas.

3.3 Validation of interpolation processes

The interpolation process was performed for both the maximum and minimum air temperatures using the methodology previously described. Table 8 shows the results of a cross-validation process performed for the interpolation results in order to evaluate the accuracy and validity of these results for the whole study area.

We used an average of about 350 pixels per image, which were selected using the proposed algorithm. Corresponding to the season of the image, the number of pixels considered ranged between 50 and 1,050 pixels for winter and summer periods, respectively. However, there are no significant deviations between the mean values of the errors for annual winter and summer periods. The values of the root mean square errors were also similar. The mean errors were less than 0.2 °C and values close to 1 °C of dispersion about the mean for both maximum and minimum temperatures.

Given the cited findings and based on the low values of these errors, it is possible to consider the interpolation process as a valid procedure to represent the spatially distributed air temperature for the whole study area. This is also consistent with the literature (Jarvis and Stuart 2001).
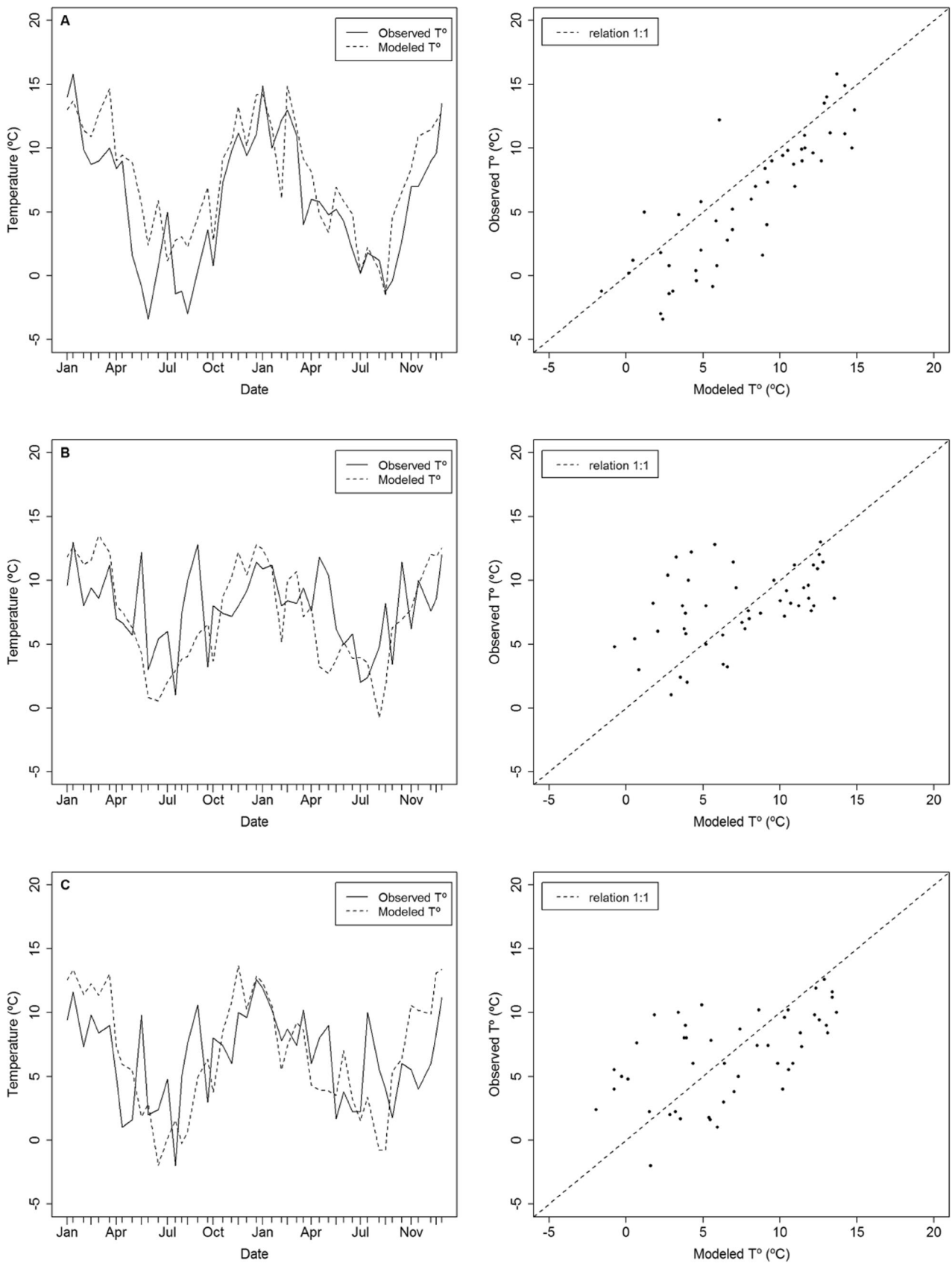
Fig. 8 Temporal distribution of minimum air temperature and the dispersion of estimated and observed values for three weather stations: **a** Rungue Embalse, **b** Melipilla, and **c** Pirque. The 1:1 *line* shows the dispersion for each data set
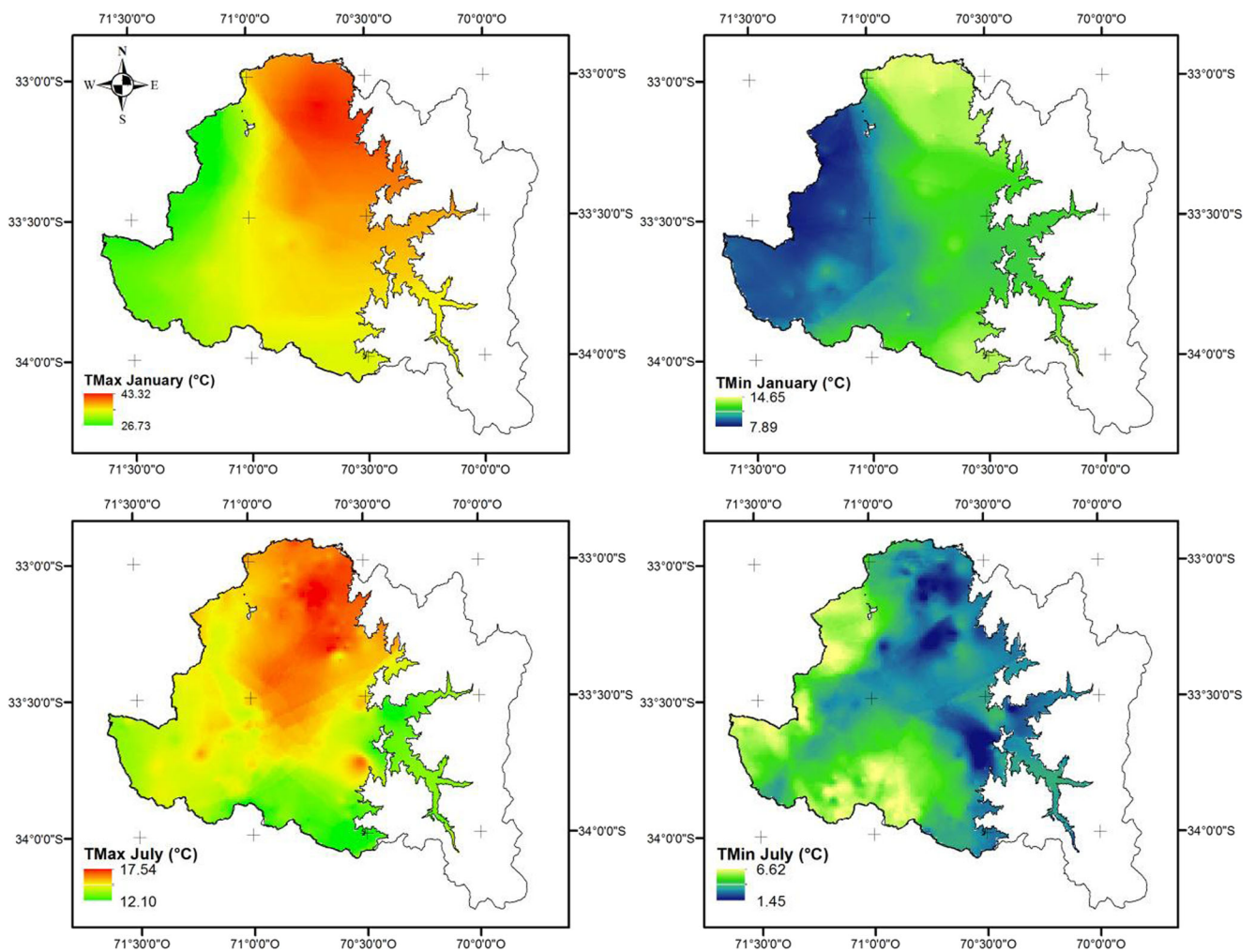
Fig. 9 Estimated maximum and minimum air temperature values for January and July for Maipo River Basin

4 Conclusions

In order to determine the daily extreme air temperatures, we developed a new methodology based on the analysis of distribution patterns of vegetation and surface temperature from

Table 8 Statistic indicators of cross-validation process for the spatial interpolation of air temperature values. Mean errors and root mean square error are reported for four seasons

	Mean errors		RMSE	
	T_{max}	T_{min}	T_{max}	T_{min}
Winter	−0.061	0.006	1.254	0.807
Fall	−0.143	0.034	1.124	0.968
Spring	−0.112	−0.017	1.890	0.573
Summer	−0.135	−0.049	1.321	0.759
Average	−0.113	−0.007	1.397	0.777

satellite imagery and independent air temperatures from meteorological stations.

After applying this methodology for determining the maximum daily air temperature, the existence of a systematic bias in the estimation of about 4 ° C was observed. This overestimation of the air temperature is due to the water stress conditions of canopy surface during periods of high temperatures in this Mediterranean ecosystem. After correcting for this bias, the model estimates did not show significant differences from the measurements obtained from standard weather stations.

A minimum temperature was corrected by adjusting a Fourier series for quantifying the minimum temperature estimated by following the cooling curve. After applying this correction, the estimates were consistently lower than the values observed at stations, highlighting those stations located in an urban context. For this situation, the information derived from pixels of vegetation around urban areas are unable to rescue the heat island effect represented by these areas, resulting in strong underestimation of the minimum temperature.

Another potential uncertainty is related to the interpolation method, for both maximum and minimum temperatures. Although cross-validation gave mean errors less than 0.1 °C and values of RMSE close to 1ºC, this source of variation must be considered when implementing the methodology and interpreting the results and leaves open the possibility of improving outcomes obtained by using other methods of interpolation such as ordinary kriging, co-kriging, or splines. Clearly, the quality of the estimates will depend on the number and conditions of pixels used for interpolation and their correct spatial coverage, particularly when applying it to a complex terrain. The main advantage of this method is the ability to increase the number of useful sources of information (via LST data), which results in better estimates particularly in cases where ground stations are scarce.

The method is able to resolve the spatial and seasonal variability as it integrates spatially distributed surface temperature information from satellite platforms. These results can then be used in mesoscale studies that seek to represent the spatial characteristics of the air temperature. The generated regional-scale air temperature information is less useful for analysis at smaller scales since it cannot resolve it at finer scales.

The methodology meets the objective of allowing a mesoscale estimation of maximum and minimum temperatures. This can be used as inter-variable in many types of models and to improve our understanding of the air temperature spatial distribution in relation to vegetation distribution.

References

Allen RG, Pereira L, Raes D, Smith M (2006) Crop evapotranspiration. FAO Irrigation and Drainage, vol. 56. FAO, Rome

Batra N, Islam S, Venturini V et al (2006) Estimation and comparison of evapotranspiration from MODIS and AVHRR sensors for clear sky days over the Southern Great Plains. Remote Sens Environ 103:1–15

Blonquist JM, Norman JM, Bugbee B (2009) Automated measurement of canopy stomatal conductance based on infrared temperature. Agric For Meteorol 149:2183–2197

Cabrera HM (2002) Respuestas ecofisiológicas de plantas en ecosistemas de zonas con clima mediterráneo y ambientes de altamontaña. Rev Chil Hist Nat 75:625–637

Campbell GS, Norman JM (1998) An introduction to environmental biophysics, 2nd edn. Springer, New York, p 286

Carlson TN, Capehart WJ, Gillies RR (1995) A new look at the simplified method for remote sensing of daily evapotranspiration. Remote Sens Environ 54:161–167

Chartzoulakis K, Psarras G (2005) Global change effects on crop photosynthesis and production in Mediterranean: the case of Crete, Greece. Agric Ecosyst Environ 106:147–157

Chuanyan Z, Zhongren N, Guodong C (2005) Methods for modelling of temporal and spatial distribution of air temperature at landscape scale in the southern Qilian mountains, China. Ecol Model 189:209–220

Colombi A, De Michele C, Pepe M, Rampini A (2007) Estimation of daily mean air temperature from MODIS LST in Alpine areas. EARSeL eProc 6:38–46

Dodson R, Marks D (1997) Daily air temperature interpolated at high spatial resolution over a large mountainous region. Clim Res 8:1–20

Duffkova R (2006) Difference in canopy and air temperature as an indicator of grassland water stress. Soil Water Res 1:127–138

Ehrler WL, Idso SB, Jackson RD, Reginato RJ (1978) Wheat canopy temperature: relation to plant water potential. Agron J 70:251

Gates DM (1968) Transpiration and leaf temperature. Annu Rev Plant Physiol 19:211–238

Geiger R (1965) The climate near the ground. Mass, Cambridge, 611

Gillies RR, Carlson TN (1995) Thermal remote sensing of surface soil water content with partial vegetation cover for incorporation into climate models. J Appl Meteorol 34:745–756

Gillies RR, Carlson TN, Cui J et al (1997) A verification of the "triangle" method for obtaining surface soil water content and energy fluxes from remote measurements of the normalized difference vegetation index (NDVI) and surface e. Int J Remote Sens 18:3145–3166

Goetz SJ (1997) Multi-sensor analysis of NDVI, surface temperature and biophysical variables at a mixed grassland site. Int J Remote Sens 18:71–94

Huete AR, Didan K, Miura T et al (2002) Overview of the radiometric and biophysical performance of the MODIS vegetation indices. Remote Sen Environ 83:195–213

Jackson RD (1981) Canopy temperature and crop water status. Adv Irrig 1:43–85

Jackson RD, Idso SB, Reginato RJ, Pinter PJ (1981) Canopy temperature as a crop water stress indicator. Water Resour Res 17:1133–1138

Jackson RD, Kustas WP, Choudhury BJ (1988) A reexamination of the crop water stress index. Irrig Sci 9:309–317

Jarvis CH, Stuart N (2001) A comparison among strategies for interpolating maximum and minimum daily air temperatures. Part II: the interaction between number of guiding variables and the type of interpolation method. J Appl Meteorol 40:1075–1084

Jiang Z, Huete AR, Chen J et al (2006) Analysis of NDVI and scaled difference vegetation index retrievals of vegetation fraction. Remote Sens Environ 101:366–378

Jones HG (1992) Plants and microclimate: a quantitative approach to environmental physiology, 2nd edn. Cambridge University Press, Cambridge, 428 p

Justice CO, Vermote E, Townshend JRG et al (1998) The moderate resolution imaging spectroradiometer (MODIS): land remote sensing for global change research. IEEE T Geosci Remote 36:1228–1249

Kawamura H, Edamatsu Y (1993) Estimation of the air temperature over the ground using AVHRR/NOAA 11. IEEE T Geosci Remote 1473–1475

Li J, Heap AD (2008) A review of spatial interpolation methods for environmental scientists. Geosc Australia, Record 2008/23

Li L, Yu Q (2007) Quantifying the effects of advection on canopy energy budgets and water use efficiency in an irrigated wheat field in the North China Plain. Agric Water Manag 89:116–122

Lookingbill T (2003) Spatial estimation of air temperature differences for landscape-scale studies in montane environments. Agric For Meteorol 114:141–151

Luebert F, Pliscoff P (2006) Sinopsis bioclimática y vegetacional de Chile. Editorial Universitaria, Santiago de Chile, p 316p

Moran M, Clarke T, Inoue Y, Vidal A (1994) Estimating crop water deficit using the relation between surface-air temperature and spectral vegetation index. Remote Sens Environ 49:246–263

Muñoz-Schick M, Moreira-Muñoz A, Villagrán C, Luebert F (2000) Caracterización florística y pisos de vegetación en los Andes de Santiago, Chile Central. B Museo Nac Hist Nat 49:9–50

Nemani RR, Running SW (1989) Estimation of regional surface resistance to evapotranspiration from NDVI and thermal-IR AVHRR data. J Appl Meteorol 28:276–284

Nieto H, Sandholt I, Aguado I et al (2011) Air temperature estimation with MSG-SEVIRI data: calibration and validation of the TVX algorithm for the Iberian Peninsula. Remote Sens Environ 115: 107–116

Pettorelli N, Vik JO, Mysterud A et al (2005) Using the satellite-derived NDVI to assess ecological responses to environmental change. Trends Ecol Evol 20:503–510

Prihodko L, Goward S (1997) Estimation of air temperature from remotely sensed surface observations. Remote Sens Environ 60:335–346

Purkey DR, Joyce B, Vicuna S et al (2007) Robust analysis of future climate change impacts on water for agriculture and other sectors: a case study in the Sacramento Valley. Clim Chang 87:109–122

R Development Core Team (2012) R: a language and environment for statistical computing. R Foundation for Statistical Computing, Vienna, Austria. ISBN 3-900051-07-0, URL http://www.R-project.org/

Sandholt I, Rasmussen K, Andersen J (2001) Derivation of a dryness index from NOAA-AVHRR data for use in large-scale hydrological modelling. Remote sensing and hydrology 2000. IAHS-AISH P, Santa Fe, pp 212–216

Sandholt I, Rasmussen K, Andersen J (2002) A simple interpretation of the surface temperature/vegetation index space for assessment of surface moisture status. Remote Sens Environ 79:213–224

Snyder W, Wan Z, Zhang Y, Feng YZ (1998) Classification-based emissivity for land surface temperature measurement from space. Int J Remote Sens 19(14):2753–2774

Stisen S, Sandholt I, Norgaard A et al (2007) Estimation of diurnal air temperature using MSG SEVIRI data in West Africa. Remote Sens Environ 110:262–274

Stisen S, Sandholt I, Norgaard A et al (2008) Combining the triangle method with thermal inertia to estimate regional evapotranspiration—applied to MSG-SEVIRI data in the Senegal River basin. Remote Sens Environ 112:1242–1255

Vancutsem C, Ceccato P, Dinku T, Connor SJ (2010) Evaluation of MODIS land surface temperature data to estimate air temperature in different ecosystems over Africa. Remote Sens Environ 114:449–465

Vitale M, Anselmi S, Salvatori E, Manes F (2007) New approaches to study the relationship between stomatal conductance and environmental factors under Mediterranean climatic conditions. Atmos Environ 41:5385–5397

Voogt JA, Oke TR (2003) Thermal remote sensing of urban climates. Remote Sens Environ 86:370–384

Wan Z, Dozier J (1996) A generalized split-window algorithm for retrieving land-surface temperature from space. IEEE T Geosci Remote 34:892–905

Wan Z, Li Z (1997) A physics-based algorithm for retrieving land-surface emissivity and temperature from EOS/MODIS data. IEEE T Geosci Remote 35:980–996

Wan Z, Zhang Y, Zhang Q, Li Z (2002) Validation of the land-surface temperature products retrieved from Terra moderate resolution imaging spectroradiometer data. Remote Sens Environ 83:163–180

Wilks DS (2005) Statistical methods in the atmospheric sciences. Academic, New York, 648 p

Yan H, Zhang J, Hou Y, He Y (2009) Estimation of air temperature from MODIS data in east China. Int J Remote Sens 30:6261–6275

Yates D, Sieber J, Purkey D et al (2005) WEAP21—a demand-, priority-, and preference-driven water planning model. Water Int 30:487–500

Zavala M (2004) Integration of drought tolerance mechanisms in Mediterranean sclerophylls: a functional interpretation of leaf gas exchange simulators. Ecol Model 176:211–226